J. Wind Eng. Ind. Aerodyn. 146 (2015) 51–58

Contents lists available at ScienceDirect

Journal of Wind Engineering and Industrial Aerodynamics

journal homepage: www.elsevier.com/locate/jweia

Simulation of turbulent flows around a prism in suburban terrain inflow based on random flow generation method simulation

Yi-Chao Li [a,*], Chii-Ming Cheng [b], Yuan-Lung Lo [b], Fuh-Min Fang [c], De-qian Zheng [d]

[a] Wind Engineering Research Center, Tamkang University, New Taipei City, Taiwan
[b] Civil Engineering, Tamkang University, New Taipei City, Taiwan
[c] Civil Engineering, National Chung-Hsing University, Taichung, Taiwan
[d] School of Civil Engineering and Architecture, Henan University of Technology, Henan, China

ARTICLE INFO

Article history:
Received 15 September 2014
Received in revised form
16 July 2015
Accepted 16 July 2015

Keywords:
Computational fluid dynamic
Atmospheric boundary layer
Large eddy simulation
Random flow generation

ABSTRACT

In the study, the modified discretizing and synthesizing random flow generation (MDSRFG) was adopted to generate an anisotropic boundary layer inlet for large-eddy simulation. The mean velocity, turbulence intensity and turbulence length scale distributions at inlet, were defined according to the measurements at TKU wind tunnel. The von Kármán model was used as the target spectrum. Wind tunnel pressure measurements on a square prism model with aspect ratio of 3 was used for validation of numerical simulation. Results show that turbulence energy is well maintained from the inlet to the downstream. The relative differences between the measurement and predicted results are 3.4% (mean drag coefficient), 11% (fluctuating drag coefficient), 25.6% (fluctuating side force coefficient) and 4.7% (Strouhal number). The simulated mean and fluctuating pressure distributions showed good agreements with the experiments. The averaged differences between measurement and predicted results are 14.49% (mean pressure coefficient) and 13.74% (fluctuating pressure coefficient). This indicates that the adoption of a reasonable process based on the MDSRFG method is an effective tool to generate a spatially correlated atmospheric boundary layer flow field.

1. Introduction

The aerodynamic behavior of a prism in an atmospheric boundary layer has been a typical problem in wind engineering. To analyze the problem numerically, an appropriate turbulent inlet flow should not only maintain its mean wind speed and the turbulence characteristics to the downstream, but also result in reliable wind force on the structure. There are several reasons to develop an appropriate procedure to generate random flow field as an inflow boundary condition in large-eddy simulations (LES). Firstly, LES has become an attractive approach due to the improvement of computational power. Secondly, the turbulence behavior within the domain is dominated by the inlet condition. Moreover, when the inlet condition is not properly prescribed, even for stationary turbulent flows, LES method could consume large execution time, such as adding artificial shear stresses or the roughness elements to obtain a target flow with fully developed turbulence.

To successfully execute this technique, several methods are available for the generation of inlet turbulence boundary-layer flow conditions. They can be classified into two general categories: precursor simulation methods and synthesis methods (Tabor and Baba-Ahmedi, 2010). Both approaches present advantages and drawbacks and can be implemented in many different ways.

Precursor simulation methods involve the generation of turbulence by conducting a pre-computation of the flow in order to generate a 'library' or database, before or in concurrency with the main LES calculation. Then, the generated fluctuations are introduced into the inlet boundary of the computational domain. Examples of this kind of approach are the methods based on cyclic domains (Liu and Pletcher, 2006; Lund et al., 1998) or those using a pre-prepared library. In particular, Lund et al. (1998) applied a modified Spalart method (Spalart and Leonard, 1985), in a concurrent library generation fashion, to sample the data as the simulation proceeds. All the above-mentioned precursor methodologies can be integrated into the main domain, sampling the turbulence in a downstream section of the inlet and then mapping it back into the inlet. In summary, the precursor simulation methods set the conditions for the LES implementation from a 'real' simulation of turbulence, it is therefore expected that the

* Corresponding author.
E-mail address: Liyichao223@gmail.com (Y.-C. Li).

http://dx.doi.org/10.1016/j.jweia.2015.07.008

velocity fluctuation field could possess many of the required statistical characteristics, including temporal and spatial correlation and energy spectrum.

Another widely used methodology is the so-called synthesized turbulence method, in which a pseudo-random coherent field of fluctuating velocities with spatial and time scales is superimposed on a predefined mean flow. The random perturbations can be generated in several different ways, such as the Fourier techniques (with its variants), the digital filter based method and the proper orthogonal decomposition (POD) analysis. An example of the Fourier approaches is the random flow generation (RFG) technique proposed by Smirnov et al. (2001) and developed on the basis of the work of Kraichnan (1970), which involves scaling and orthogonal transformations applied to a continuous flow field. This transient flow field is generated in a three-dimensional domain as a superposition of harmonic functions with random coefficients. This method can generate an isotropic divergence-free fluctuating velocity field satisfying the Gaussian' s spectral model as well as an inhomogeneous and anisotropic turbulence flow, provided that an anisotropic velocity correlation tensor is given. Smirnov et al. (2001) used their approach to set inlet boundary conditions to LES methods in the simulation of turbulent fluctuations in a ship wake as well as initial conditions in the simulation of turbulent flow around a ship-hull. Another successful application was the particle dynamics modeling by Smirnov et al. (2005). By adopting the concepts of the RFG method, Huang et al. (2010) made further improvements and proposed the discretizing and synthesizing random flow generation (DSRFG) method to produce an inlet fluctuating velocity field that meet specific spectrum. Castro et al. (2011) then modified the DSRFG to MDSRFG by preserving the statistical quantities at the inlet part of the computation domain and keeping independence of number of points for simulating target spectrum. However, few studies investigated and successfully maintained statistical quantities of the turbulence boundary layer from inlet to the downstream in the computation domain. Therefore, there are still some technical and theoretical problems, such as the adjustment of spatial correlation and the definitions of anisotropic turbulence intensity and turbulence length scale, to be overcome.

Accordingly, this paper attempts to generate the suburban terrain inlet by MDSRFG. The related parameters, such as the mean wind speed, turbulence intensity, turbulence integral scale and power spectra from the suburban turbulent boundary layer flow are provided from Tamkang University BLWT-1(TKU BL-1) wind tunnel tests. A prism model with an aspect ratio of 3 was built; and pressure data was measured in a suburban terrain flow field to validate the numerical results.

2. Method

2.1. Wind tunnel experiment

In order to assure the reliability of the turbulence boundary inlet based on MDSRFG for large-eddy simulations, a prism model (see Fig. 1) with a characteristic length $D=0.1$ m is set and tested in a wind tunnel with a test section of 18 m$(L)\times 2$ m$(W)\times 1.5$ m (H). The turbulent boundary layer inlet flow with a power-law α value of 0.25 is generated to represent wind profiles over a suburban terrain. The freestream velocity (U_δ) of the approach flow is 8.85 m/s. The boundary layer thickness (δ) is 1 m. The corresponding Reynolds number ($U_\delta D/\nu$) is 5.9×10^4. The aspect ratio (h/D) of the square pressure model is 3. The total measurement period is 280 s with a sampling rate of 200 Hz.

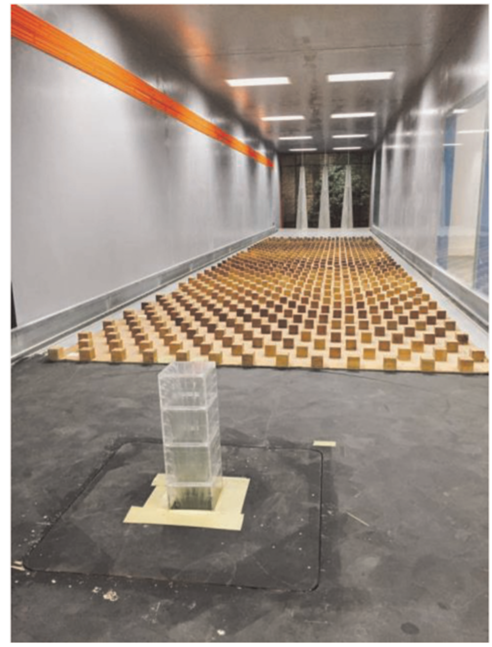

Fig. 1. Pressure model in TKU BL-1 with suburban terrain.

2.2. Numerical method

The simulation adopts the weakly-compressible-flow method (Song and Yuan, 1988). The continuity and momentum equations are

$$\frac{\partial p}{\partial t} + \nabla\cdot\left(k\vec{V}\right) = 0 \tag{1}$$

$$\frac{\partial \vec{V}}{\partial t} + \vec{V}\cdot\nabla\vec{V} = -\nabla\frac{p}{\rho} + \nabla\cdot\left[(\nu+\nu_t)\nabla\vec{V}\right] \tag{2}$$

where p, $\overrightarrow{V}$ and t denote respectively pressure, velocity and time; k is the bulk modulus of elasticity of air; ν and ν_t are respectively the laminar and turbulent viscosities. The turbulent viscosity (ν_t) is determined based on a subgrid-scale turbulence model as

$$\nu_t = C_S\Delta^2\left(\frac{S_{ij}^2}{2}\right)^{0.5} \tag{3}$$

where C_S is the Smagorinsky coefficient; Δ denotes the characteristic length of the computational grid and $S_{ij} = (\partial u_j/\partial x_i + \partial u_i/\partial x_j)$. Based on a concept of dynamic model proposed by Germano et al. (1991), two grid systems, corresponding respectively to a grid filter and a test filter, are used in the flow calculations. The test filter width is selected as twice of the grid filter width. By comparing the resulting differential turbulent shear stresses associated with the two filter systems at a certain time step in the computation, the C_S value at the next time step is then obtained. The dynamically determined C_S is clipped at zero and 0.23.

A finite-volume method is adopted to calculate and then update the fluxes within each elapsed time based on an explicit predictor-corrector scheme (MacCormack, 1969). Second-order accuracy in space is used in the discretized equations of Eqs. (1) and (2), and the Crank–Nicolson scheme is used in time integration. During the computation process, the time increment is limited by the Courant–Friedrichs–Lewy (CFL) criterion (Courant et al., 1967).

The Courant number is chosen as 0.4 to ensure that the computation converges at each time step. In this study, by considering the limitation of CFL criterion, the normalized time intervals ($\Delta T = \Delta t U_\delta / D$) are larger than 0.0035 in the first 10 s flow computation and then fixed at 0.003 for the subsequent computations.

2.3. Synthesizing method

Derivation of the MDSRFG method and the associated validations can be referred to the work by Castro et al. (2011). A brief formulation of the method is presented as follows:

$$u(x,t) = \sum_{m=1}^{M}\sum_{n=1}^{N}\left[a_i^{m,n}\cos\left(\tilde{k}_j^{m,n}\tilde{x}_j + \omega_{m,n}\frac{t}{\tau_0}\right) + b_i^{m,n}\sin\left(\tilde{k}_j^{m,n}\tilde{x}_j + \omega_{m,n}\frac{t}{\tau_0}\right)\right] \tag{4}$$

$$a_i^{m,n} = \mathrm{sign}\left(r_i^{m,n}\right)\sqrt{\frac{4c_i}{N}E_i\left(k_m\right)\Delta k_m\frac{\left(r_i^{m,n}\right)^2}{1+\left(r_i^{m,n}\right)^2}} \tag{5}$$

$$b_i^{m,n} = \mathrm{sign}\left(r_i^{m,n}\right)\sqrt{\frac{4c_i}{N}E_i\left(k_m\right)\Delta k_m\frac{1}{1+\left(r_i^{m,n}\right)^2}} \tag{6}$$

where $\omega_{m,n} \in N(0, 2\pi f_m)$; $r_i^{m,n}$ is a three dimensional normal distributed random number with $\mu_r = 0$ and $\sigma_r = 0$. $c_i = 0.5\bar{U}$, and $\bar{U}$ is the local mean wind speed. $\tilde{x} = x/L_s$, and $L_s = \theta_1\sqrt{L_u^2 + L_v^2 + L_w^2}$ (the scaling factor for spatial and time correlation). $\tau_0 = \theta_2 L_s/\bar{U}$ is the parameter introduced to allow for the control over the time correlation. The turbulence kinetic energy $\tilde{k}^{m,n} = \mathrm{k}^{m,n}/k_0$ is the three dimensional distribution on the sphere of inhomogeneous and anisotropic turbulence.

The auto-correlation function can be computed by the mathematical manipulation from Eq. (4)

$$\overline{u(x,t)u(x,t+\tau)} = \frac{2c}{N}\sum_{m=1}^{M}\sum_{n=1}^{N}E\left(k_m\right)\Delta k_m\cos\left(\frac{\tau}{\tau_0}\omega_{m,n}\right) \tag{7}$$

The auto-correlation coefficients are dominated by the frequency segments (Δk_m) and time correlation parameter θ_2. An expression for the spatial correlation can be obtained in an analogous way as

$$u(x,t)u(x',t) = \frac{2c}{N}\sum_{m=1}^{M}\sum_{n=1}^{N}E\left(k_m\right)\Delta k_m\cos\left[\tilde{k}_j^{m,n}\frac{\left(x_j' - x_j\right)}{L_s}\right] \tag{8}$$

Both of the above equation shows that the spatial correlation and auto-correlation are controlled by L_s, and are used in the spectrum $E(k_m)$.

2.4. Computation domain and meshes

The simulation domain for the present study is 33D in the longitudinal (x) direction ($-5 < x/D < 28$), 16D in the lateral (y) direction, and 10D in the vertical (z) direction, where D is the width of the prism model. In this study, two typical cases are established, which are respectively an empty test section (without the prism) and including a prism with $h/D=3$ setting at $x/D=4$. The blockage ratio of the prism case is less than 2%. In both cases, 3-D computations are performed. According to AIJ guidelines and COST (European Cooperation in the Field of Scientific and Technical Research) (Yoshihide et al., 2008), the selected height of the computational domain is lower than a recommended value of 6 h. To observe the blockage effect, the preliminary examinations are made and found that the mean velocity contours and stream lines near the top boundary of the computational domain appear parallel to the boundary surface, which implies that the blockage effect due to the prism is insignificant.

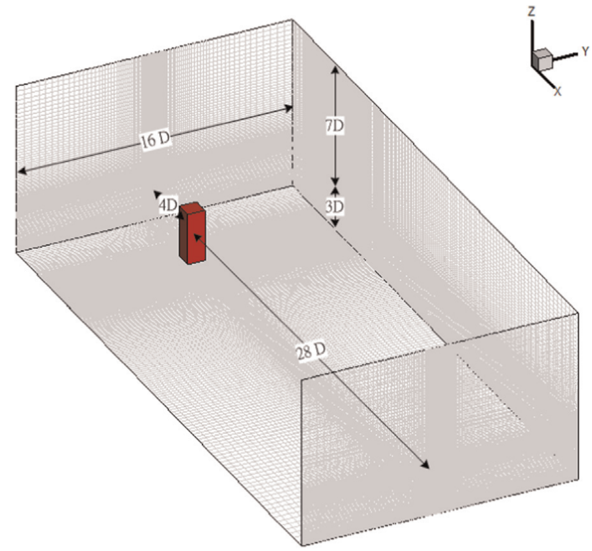

Fig. 2. Computation domain and grid system.

Fig. 2 shows the computation domain and the corresponding mesh system. The closest grid point near the prism surface is adopted to be 0.025D, with corresponding wall unit y^+ ranging from about 8–30 ($y^+ = u_* y/\nu$; u_* is the friction velocity). The grid is non-uniformly distributed and is set with caution to avoid large stretching in the neighborhood region of the prism model to reduce cut-off error of wave number in LES. In the y-direction, 40 nodes are distributed in the left and right domains with a stretching ratio of 1.05. In the x-direction, 40 nodes are distributed non-uniformly from the inlet to the windward surface of the prism model with a stretching ratio of 1.03. In the wake zone of the computational domain, a grid size of 0.05B is used near the prism leeward surface and 148 nodes are used with a stretching ratio of 1.02. In the z direction, 100 nodes are distributed with the points clustered near the ground and the top surface of the prism (stretching ratio of 1.02). Totally, about 2,500,000 grid elements are used in the present simulation ($250 \times 100 \times 100$).

2.5. Boundary conditions

Appropriate values of pressures and velocities are specified at exterior cells (or phantom cells) to reflect the correct physical nature of the boundaries. No-slip conditions are set at the ground and the prism surfaces. The top, both sides and downstream boundaries are set by zero-gradient conditions (in the directions normal to the boundaries for both the velocities and pressures).

The upstream boundary condition is generated by the MDSRFG method. The inhomogeneous anisotropic turbulent conditions of the suburban terrain field are created in this study. Basically, the result of experimental u-component spectrum agrees with the von Kármán spectrum. Although the spectra of the v- and w- components are not available in experiments, the von Kármán spectra are considered good models to describe anisotropic atmospheric boundary layer flows, defined as

$$\text{u - component: } S_u(f) = \frac{4\left(I_u\bar{U}\right)^2\left(L_u/\bar{U}\right)}{\left[1 + 70.8\left(fL_u/\bar{U}\right)^2\right]^{5/6}} \tag{9}$$

$$\text{v - component: } S_v(f) = \frac{4\left(I_v\bar{U}\right)^2\left(L_v/\bar{U}\right)\left[1 + 188.4\left(2fL_v/\bar{U}\right)^2\right]}{\left[1 + 70.8\left(2fL_v/\bar{U}\right)^2\right]^{11/6}} \tag{10}$$

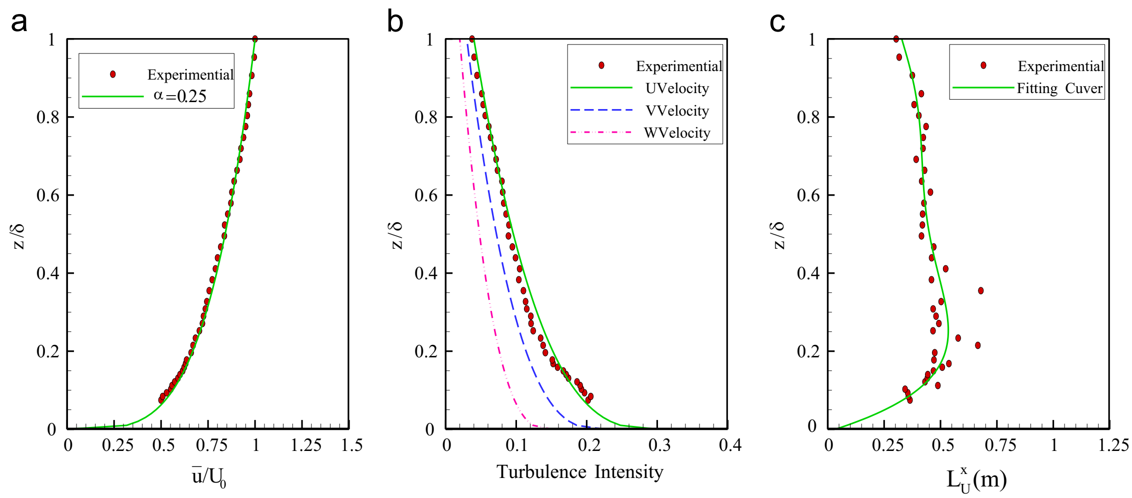

Fig. 3. Vertical profiles of inlet condition (a) mean wind speed, (b) turbulence intensity and (c) integral length scale.

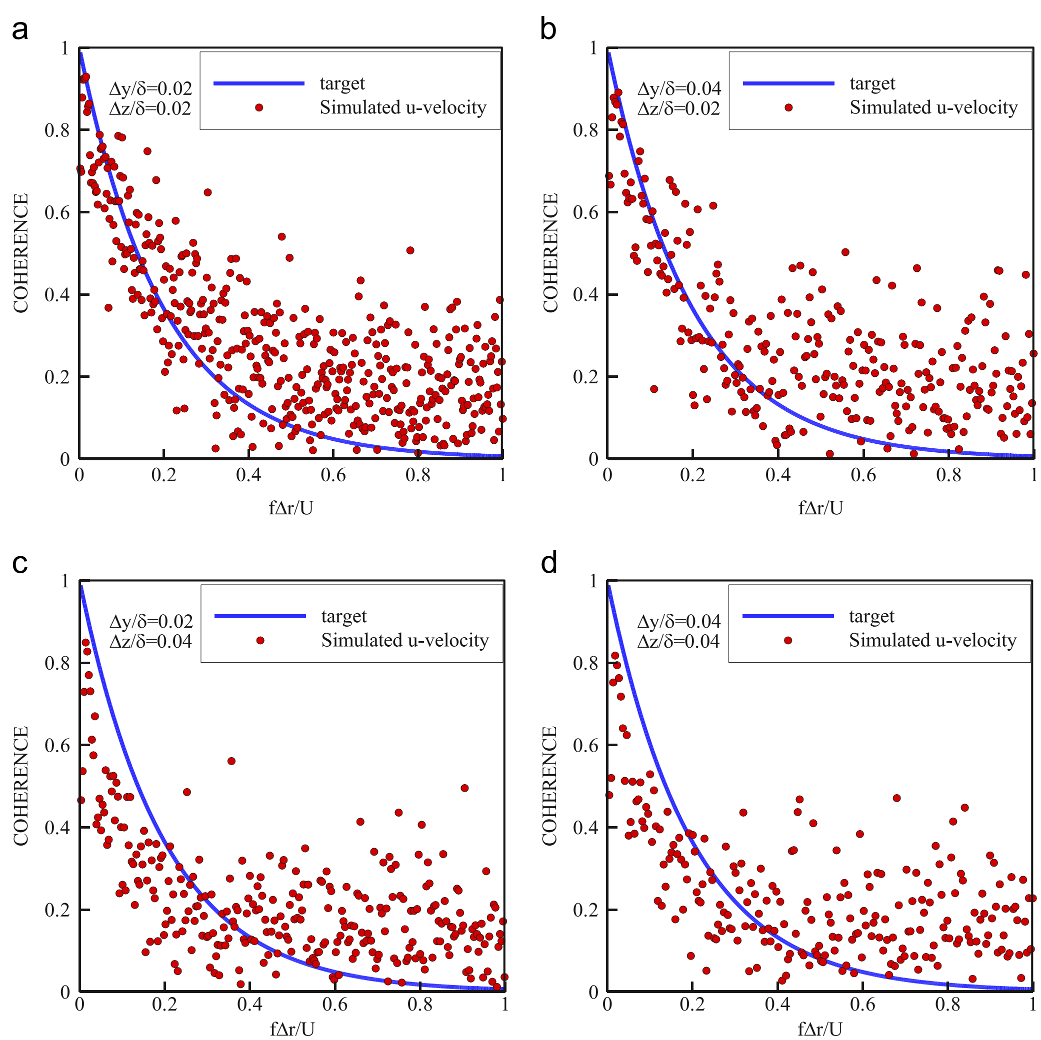

Fig. 4. Cross coherence at **z/δ**=0.5 with θ_1=5.5, the dimensionless length $\Delta r = \sqrt{\Delta y^2 + \Delta z^2}$ (a) $\Delta y/\delta$=0.02 $\Delta z/\delta$=0.02, (b) $\Delta y/\delta$=0.04 $\Delta z/\delta$=0.02, (c) $\Delta y/\delta$=0.02 $\Delta z/\delta$=0.04, (d) $\Delta y/\delta$=0.04 $\Delta z/\delta$=0.04.

w – component: $S_w(f)$

$$= \frac{4\left(I_w\bar{U}\right)^2\left(L_w/\bar{U}\right)\left[1+188.4\left(2fL_w/\bar{U}\right)^2\right]}{\left[1+70.8\left(2fL_w/\bar{U}\right)^2\right]^{11/6}} \tag{11}$$

All the prescribed parameters are obtained from TKU BL1 wind tunnel experiments. Regarding the u-component velocity measurements, the total measurement period is 60 s with a sampling rate of 500 Hz. The mean wind speed profile is set to follow the power law with α=0.25. The longitudinal turbulence intensity profile is set by $I_u = 0.3 - 0.26(z/\delta)^{0.35}$. The longitudinal length scale (L_u) is determined by integrating the space correlation coefficient of wind speeds in the longitudinal direction and its vertical profile can be regressed by a six-order polynomial form

$$L_u = \int_0^{\infty} \rho_{12}(\Delta r)d\Delta r \tag{12}$$

where $\rho_{12}(\Delta r)$ represents the normalized correlation coefficient function of wind speeds u_1 and u_2 with a distance of Δr. The calculation of the length scale L_u is based on the measured time series at a typical location in wind tunnel test with Taylor hypothesis, instead of measuring spatial correlation.

Due to the lack of the available turbulence information regarding the v- and w- components, the turbulence intensities in the other two directions are taken as $I_v = 0.75I_u$ and $I_w = 0.5I_u$, and the turbulence length scales (L_v and L_w) are both assumed to be $0.5L_u$ (Engineering Sciences Data Unit, 1985; Farell and Iyengar, 1999). The experimental and the adopted curve-fitted profiles are shown in Fig. 3.

Before synthesizing the wind speed of the inlet, it is important to determine the appropriate spatial parameter (θ_1) and the time

Table 1
MDSRFG parameters for suburban terrain.

N	M	K_0	θ_1	θ_2
100	2000	0.01	5.5	0.2

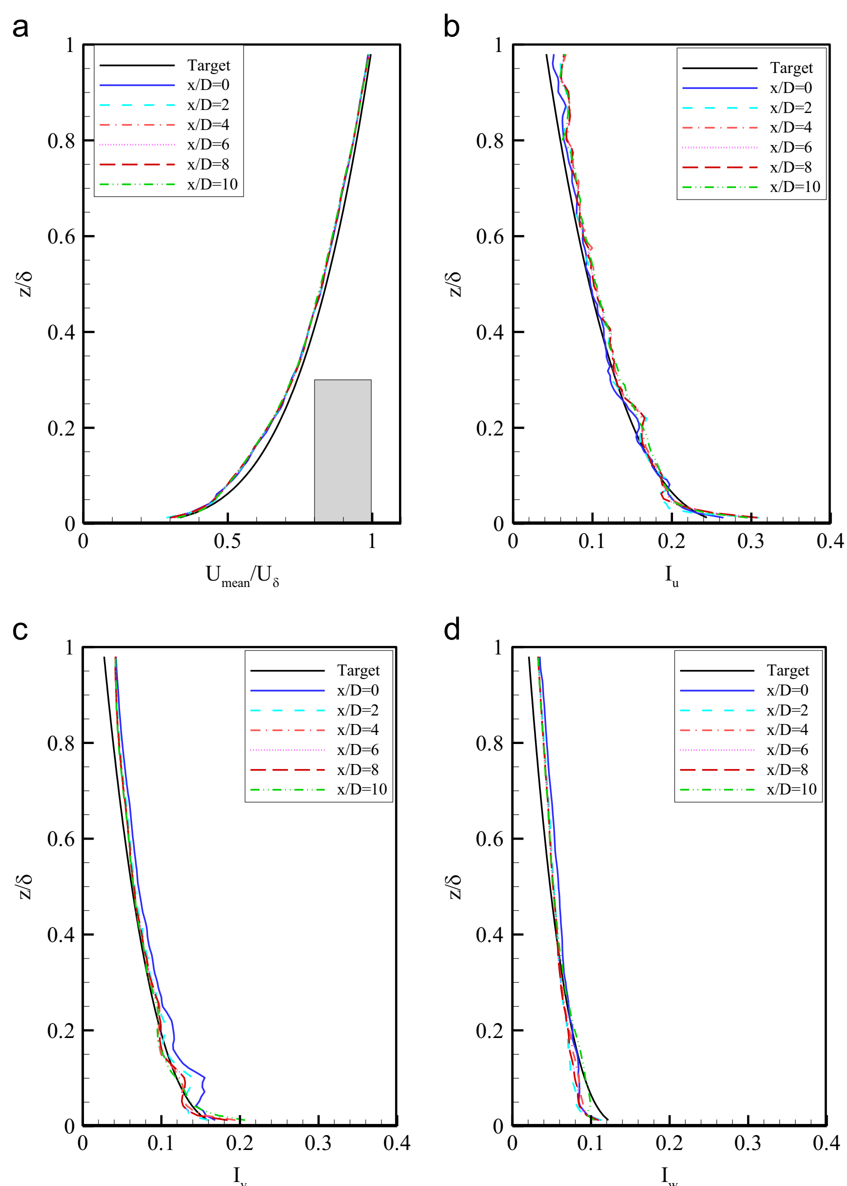

Fig. 5. Comparison of mean velocity and turbulence intensity from inlet to x/D=10 with target profiles. (a) Mean wind speed, (b) turbulence intensity of u-component, (c) turbulence intensity of v-component, (d) turbulence intensity of w-component.

parameter (θ_2). θ_1 dominates the scaling factor according to the definition in Section 2.3, influences the spatial and time correlation. Although Eq. (8) gives a convenient way to estimate the spatial correlation between the synthesizing points having the same form of spectra, the turbulence boundary layer spectra vary significantly along the vertical direction. In order to define the spatial correlation to determine θ_1, a theoretical equation for reference, the spatial coherence proposed by Davenport (1968), is adopted to be the target function as

$$Coh = e^{-\hat{f}}, \hat{f} = \frac{n\left[C_z^2(z_1 - z_2)^2 + C_y^2(y_1 - y_2)^2\right]^{1/2}}{0.5\left[U(z_1) + U(z_2)\right]} \tag{13}$$

where y_1, y_2, z_1, z_2 are the coordinates on the y–z plane. C_y and C_z are the exponential decay coefficients in the horizontal and vertical direction respectively. $C_z = 10$ and $C_y = 16$ are suggested by Davenport (1968) and are consistent with the results of TKU BL1 suburban terrain. The experimental coherence function is obtained from calculating the cross spectrum of two simultaneously recorded wind speeds, which is defined as

$$S_{12}(\Delta r, f) = S_{12}^C(\Delta r, f) + iS_{12}^Q(\Delta r, f) \tag{14}$$

where the real part is known as the co-spectrum and the imaginary part is quadrature spectrum. The coherence function is then defined as

$$Coh(\Delta r, f) = \sqrt{\frac{\left[S_{12}^C(\Delta r, f)\right]^2}{S_1(f)S_2(f)} + \frac{\left[S_{12}^Q(\Delta r, f)\right]^2}{S_1(f)S_2(f)}} \tag{15}$$

where $S_1(f)$ and $S_2(f)$ are auto-spectra of wind speeds u_1 and u_2 respectively.

In the boundary layer flow field, since the most significant variations of turbulence intensity and turbulence integral length scale occur in the vertical direction, the adjustment of θ_1 is therefore conducted to fit the vertical coherences according to the theoretical function. Fig. 4 illustrates the resulting coherence values at various horizontal and vertical positions as $\theta_1 = 5.5$. It can be seen that the general tendency of the coherence variations appears consistent with target curve.

θ_2 is the parameter introduced to allow for some control over the auto-correlation, therefore θ_2 can adjust the turbulence integral length scale determining by Eq. (7) to correspond (match the) original setup. All MDSRFG parameters related to the spatial correlation and time correlation for suburban terrain flow field are listed in Table 1.

3. Results

3.1. Velocity profiles and spectra

To examine the suburban terrain inlet flow generated according to the MDSRFG, flow simulations are conducted in an empty test section at the beginning. The turbulent flow field is generated with a sampling frequency of 200 Hz. Both the total generating time

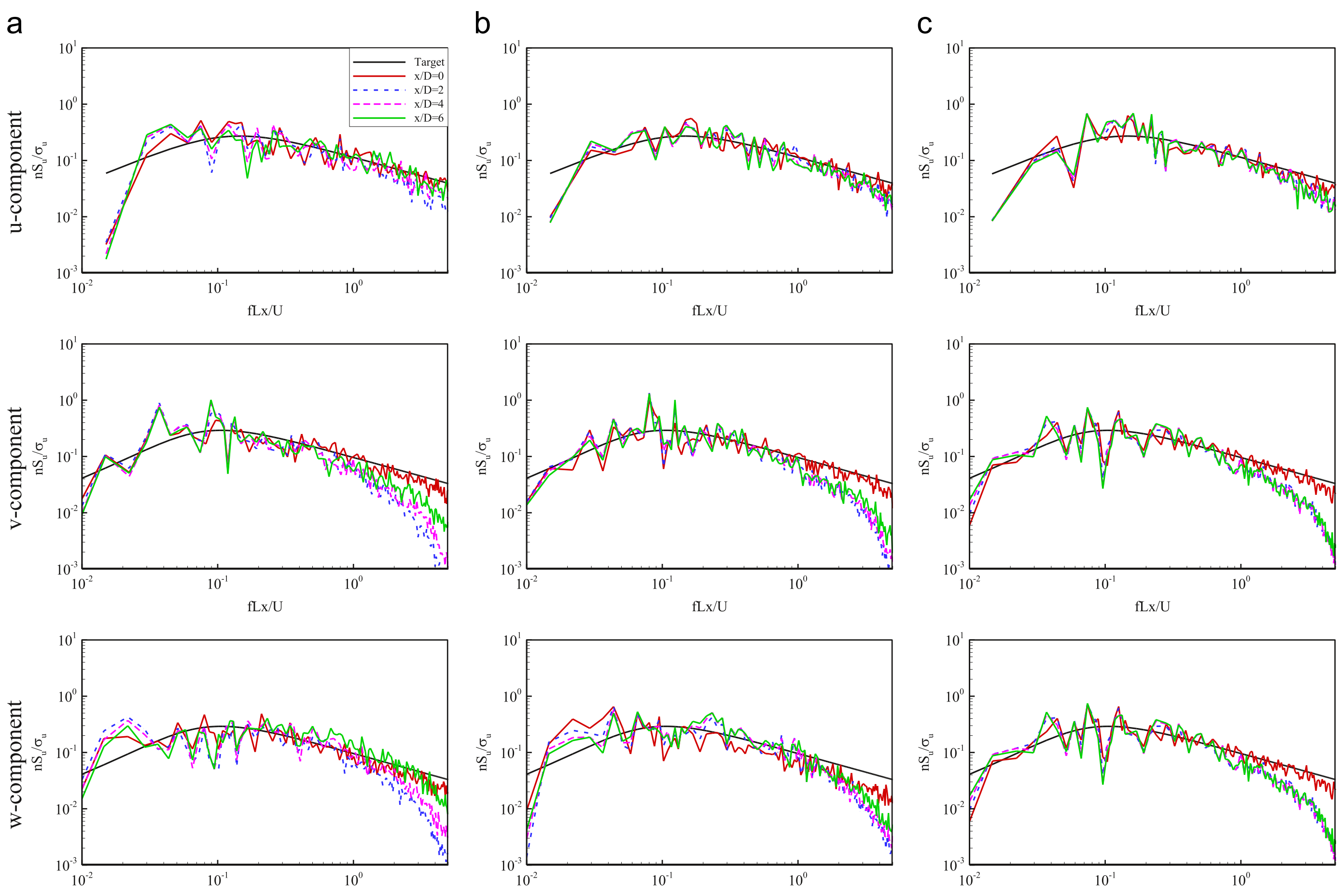

Fig. 6. Comparison of the 3-components power spectra. (a) $z/\delta = 0.25$, (b) $z/\delta = 0.5$ and (c) $z/\delta = 0.75$.

and simulation time duration are 280 s, the corresponding normalized period ($T = tU_\delta/D$) is 24780.

Based on the numerical results, Fig. 5(a) shows that the mean wind speed profile maintain fairly well from the upstream cross section to that at $x/D=10$. The power-law α value at various cross sections remain to be 0.25. Fig. 5(b)–(d) depict respectively the turbulence intensity profiles from inlet to the downstream ($x/D=10$). The I_u profile generated by the MDSRFG ($x/D=0$) agrees well with the target as prescribed (see Section 2.4) and the u-component turbulence can maintain its turbulence energy even at $x/D=10$. On the other hand, although the I_v profile at the inlet ($x/D=0$) is slightly over-predicted within the range from $z/\delta=0.05$–0.2, the profiles at the other cross sections are self-adjusted by the sub-grid turbulence and are in good agreement with the target profile. The I_w profiles appear also consistent with the target one with a slight decay near the ground region. Since a symmetric boundary condition is used at the top boundary of the computation domain, all of the turbulence intensity profiles appear a little bit overestimated near $z/\delta=1$ in the domain. The outcome can be improved by extending the computation in the vertical direction.

The results of three components power spectra at three different heights ($z/\delta=0.25$, 0.75, 0.5) and four longitudinal positions ($x/D=0$, 2, 4, 6) are shown in Fig. 6. At inlet ($x/D=0$), turbulence spectra match well with the target spectra. The u-component spectra at $x/D=2$, 4, 6 are also in good agreement with target value. The v- and w-components spectra generally agree well with the target ones. However, the energy starts to decay as the reduced frequency (fL_x/U) exceeds 1. This may attribute to the reason that the assumed v- and w-component length scale profiles are smaller than the u-component length scale profile. As a result, the part of high-frequency energy from small-scale turbulence eddies cannot be well maintained in the larger computational grid size. However, further investigations should be carried out in the future to verify this argument. Nevertheless, the turbulence energy losses of the two components are minor, and the preservation of turbulence energy of u-component is the major control of the wind load on the prism.

3.2. Aerodynamic characteristic

Table 2 illustrates the comparison between the numerical and experimental results in terms of the mean drag coefficient ($\bar{C_D} = \bar{F_x}/0.5\rho U_h^2 Dh$), fluctuating drag coefficient ($C_D' = F_x'/0.5\rho U_h^2 Dh$), fluctuating side force coefficient ($C_L' = F_y'/0.5\rho U_h^2 Dh$) and Strouhal number ($n_{peak}D/U_h$) of the prism. The predicted $\overline{C_D}$ and Strouhal number are close to the wind tunnel measurements. The fluctuating aerodynamic coefficients (C_D' and C_L') are 11–25% under-predicted.

Fig. 7 also shows the comparison of the mean and root-mean-square surface pressure coefficient distributions ($\overline{C_p} = \overline{p}/0.5\rho U_h^2$; $C_p' = p'/0.5\rho U_h^2$) on the center vertical plane ($y/D=0$). The predicted $\overline{C_p}$ distributions on the windward and leeward surfaces of the prism are close to the experimental results. In terms of C_p', the fluctuating pressure on the windward surface appears to be well predicted, the maximum different is about 11% near top of the prism. However, about 30% over-predictions are found in the leeward part. The averaged differences between measurement and predicted results are 14.5% (mean pressure coefficient) and 13.7% fluctuating pressure coefficient).

Table 2
Comparisons of aerodynamic coefficients.

	Experimental	*Numerical*	*Relative difference* (%)
$\bar{C_D}$	0.853	0.882	3.4
C_D'	0.228	0.203	11.0
C_L'	0.203	0.151	25.6
Strouhal number	0.085	0.089	4.7

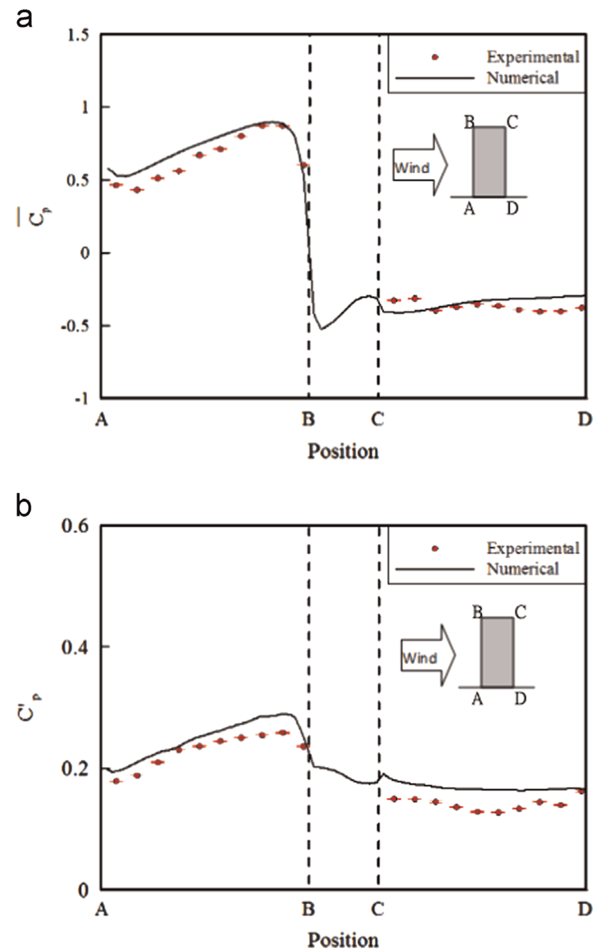

Fig. 7. Comparisons of surface pressure on the prism (a) $\overline{C_p}$ (b) C_p'.

4. Conclusions

In this study, the MDSRFG is adopted to generate the inlet boundary condition of the suburban terrain flow field for large-eddy simulation. The simulated mean wind speed profile, turbulence intensity profile and power spectra of velocity fluctuations agree fairly well to the target values. The results indicate that most of the eddy turbulence energy maintains quite well even to the downstream. The parameters of spatial and time correlations are adjusted by wind tunnel results and theoretical equations to show that the MDSRFG method is an effective numerical tool to generate a spatially correlated atmospheric boundary layer flow field. The simulated turbulent boundary layer was then applied on a square prism, and the simulated prism aerodynamics is also in good agreement with the wind tunnel measurements. This process can be extended to generate turbulent boundary layer approaching flows subject to different terrains for further numerical studies.

Reference

Castro, H.G., Paz, R.R., Sonzogni, V.E., 2011. Generation of turbulence inlet velocity conditions for large eddy simulation. Mec. Comput. XXX, 2275–2288.

Courant, R., Friedrichs, K.O., Lewy, H., 1967. On the partial difference equations of mathematical physics. IBM J. 11, 215–234.
Davenport, A.G., 1968. The dependence of wind load upon Meteorological Parameter. In: Proceedings of International Research Seminar on Wind Effects on Buildings and Structures. University of Toronto Press, Toronto, pp. 19–82.
Engineering Sciences Data Unit, 1985. Characteristics of Atmospheric Turbulence Near the Ground. ESDU International Ltd, London, Data Item 85020.
Farell, C., Iyengar, K.S., 1999. Experiments on the wind tunnel simulation of atmospheric boundary layers. J. Wind Eng. Ind. Aerodyn. 79, 11–35.
Germano, M., Piomelli, U., Moin, P., Cabot, W.H., 1991. A dynamic subgrid-scale eddy viscosity model. Phys. Fluids 3, 1760–1765.
Huang, S.H., Li, Q.S., Wu, J.R., 2010. A general inflow turbulence generator for large eddy simulation. J. Wind Eng. Ind. Aerodyn. 98, 600–617.
Kraichnan, R.H., 1970. Diffusion by a random velocity field. Phys. Fluids 13, 22–31.
Liu, K.L., Pletcher, R.H., 2006. Inflow conditions for the large eddy simulation of turbulent boundary layers: a dynamic recycling procedure. J. Comput. Phys. 219 (1), 1–6.
Lund, T.S., Wu, X., Squires, K.D., 1998. Generation of turbulent inflow data for spatially-developing boundary layer simulations. J. Comput. Phys. 140, 233–258.
MacCormack, R. 1969. The effect of viscosity in hyper-velocity impact cratering. AIAA Paper, pp. 69–354.
Smirnov, A., Celik, I., Shi, S., 2005. Les of bubble dynamics in wake flows. Comput. Fluids 34, 351–373.
Smirnov, R., Shi, S., Celik, I., 2001. Random flow generation technique for large eddy simulations and particle-dynamics modeling. J. Fluids Eng. 123, 359–371.
Song, C., Yuan, M., 1988. A weakly compressible flow model and rapid convergence methods. J. Fluids Eng. 110 (4), 441–455.
Spalart, P.R., Leonard, A., 1985. Direct numerical simulation of equilibrium turbulence boundary layer. In: Proceedings of the 5th Symposium on Turbulent Shear Flows. Ithaca, NY.
Tabor, G., Baba-Ahmedi, M., 2010. Inlet conditions for large eddy simulation: a review. Comput. Fluids 39, 553–567.
Yoshihide, T., Akashi, M., Ryuichiro, Y., Hiroto, K., Tsuyoshi, N., Masaru, Y., Taichi, S., 2008. AIJ guidelines for practical applications of CFD to pedestrian wind environment around buildings. J. Wind Eng. Ind. Aerodyn. 96, 1749–1761.